RSC Advances

ROYAL SOCIETY OF CHEMISTRY

www.rsc.org/advances

Synthesis and evaluation of the targeted binding of RGD-containing PEGylated-PEI/DNA polyplex micelles as radiotracers for a tumor-targeting imaging probe

Adhimoorthy Prasannan[1, 4], Tilahun Ayane Debele[1] Hsieh-Chih Tsai[1,*], Chiz -Cheng Chao[2], Che-Ping Lin[3], Ging-Ho Hsiue[3,4]*

1. Graduate Institute of Applied Science and Technology, National Taiwan University of Science and Technology, Taipei 106, Taiwan, ROC.
2. Department of Chemical Engineering, National Chung Hsing University, Taichung, 402, Taiwan, ROC.
3. Department of Chemical Engineering, National Tsing Hua University, Hsinchu, 320, Taiwan, ROC.
4. Department of Chemical Engineering/R&D Center for Membrane Technology, Chung Yuan University, Chung Li, 320, Taiwan, ROC.

[*] To whom correspondence and reprint requests should be addressed.

Prof. Hsieh-Chih Tsai

E-mail:h.c.tsai@mail.ntust.edu.tw

Tel.:+886-2-27303625, Fax:+886-2-27303733

Prof. Ging-Ho Hsiue

E-mail: ghhsiue@mx.nthu.edu.tw

Tel.: + 886-3-5719956, Fax: + 886-3-5726825

Key Words

Imaging probe, Targeted binding, Polyplex, Radiotracers, Gene delivery

Abstract

Site-specific labeling of molecular imaging probes necessitates the topical administration of medications during the development of homogeneous tracers. Hence, receptor-mediated gene transfer is believed to be of enormous significance in the clinical translation of a promising gene delivery technique. Plasmid DNA (*p*EGFP) and polycations produce polyplexes, which can be proficient probes for molecular imaging when accompanied by a gamma emitter. Therefore, this study describes the physico-biological characterization of a radiotracer for tumor imaging in a HeLa tumor-bearing mouse model. Polyplex micelles were formed with *p*EGFP and Arg-Gly-Asp (RGD) peptide-modified poly(ethylene glycol)-grafted polyethylenimine (E[c(RGDyK)]$_2$-PEG-*g*-PEI) and were labeled with ^{99m}Tc for the *in vivo* study. The various PEG-*g*-PEIs prepared by controlling the PEG-to-PEI ratios were confirmed by ^{1}H-NMR. The sizes and zeta potentials of the PEG-*g*-PEI/DNA polyplexes were 90-135 nm and 40-50 mV, respectively. The biophysical characterization of *p*EGFP in polyplexes was evaluated via various methods, including determination of the condensation efficiency of the polymers and the biodistribution, *in vitro* stability, *in vivo* application, and kinetics of the radiolabeled polyplexes. These characteristics were studied as a function of time using 3D-SPECT/CT images and by end-point scintillation counting. The polyplex of PEG-*g*-PEI/DNA fabricated with a PEG/PEI ratio of 10:1 and N/P=1, i.e., PP10/D, exhibited the lowest cytotoxicity and the highest transfection efficiency. The cyclic-RGD peptide-modified polyplex PEG-*g*-PEI/DNA (RPP10/D) had significantly higher binding affinity and transfection efficiency than the non-targeting PP10/D did. ^{99m}Tc radio-labeled PP10/D and RPP10/D had prepared with high radiolabeling efficiency of greater than 95% and radiochemical stability above 80%, both in saline and in rat plasma, when stored for 24 h and was evaluated for its tumor-targeting capability and biodistribution. Through *in vivo*

SPECT/CT images, it was determined that RPP10/D-^{99m}Tc presented higher uptake in the tumor than PP10/D-^{99m}Tc at all of the post-injection times studied. We found that the two tracers of radioactive complexes mainly accumulated in the liver, spleen and kidneys at 24 h after intravenous injection in female BALB/c nude mice bearing subcutaneous HeLa tumors. The accumulation of the site-specifically labeled RPP10/D-^{99m}Tc was lower in liver, kidney and spleen compared with non-targeting PP10/D-^{99m}Tc.

Introduction

The introduction of a genetic substance into human diseased cells is a severe bottleneck in the progress of gene delivery for many clinical applications.[1, 2] An appropriate gene delivery system is a prerequisite for cellular uptake; the transfer of large hydrophilic and charged molecules through the cellular membrane of living cells is hampered, and the undesirable extracellular circumstances provide vast opportunities to degrade DNA.[3] Although the efficiencies of DNA condensation and decondensation are of significant importance in gene delivery progress, a vector's biocompatibility is also an essential factor.[4] Thus, the formation of DNA condensates has been induced by the addition of non-viral carriers *in vitro* such as metal cations, cationic polymers, liposomes, peptides and polyamines.[5-7] Synthetic cationic polymers have been widely studied as a major group of non-viral carriers.[8] Hitherto, polyethylenimine (PEI) has been considered the most potent non-viral gene carrier for both *in vitro* and *in vivo* administration.[9] However, the toxicity of PEI has been the chief drawback in its application.[10] The enhancement of DNA condensation and DNA release has been achieved by combining two condensing agents while preparing the polyplex, which also provides lower cytotoxicity compared to when PEI is used as the sole condensing agent.[11]

In particular, poly(ethylene glycol)-modified (PEGylated) PEI-based polyplexes are promising for *in vivo* gene therapy applications as potential non-viral vectors.[12] They are formed through a self-assembled electrostatic interaction between plasmid DNA (*p*EGFP) and PEG-*b*-polycation copolymers and are configured as polyplex micelles with a core-shell structure.[13] The outer hydrophilic PEG segments enhance the micelle stability in serum, inhibits aggregation of polyplex, reduce protein opsonization of polyplex, improve the pharmacokinetic properties, and reduce the toxicity.[13, 14] Recently, cyclic RGD peptides [c(RGDyK)] were incorporated onto the

surface of the polyplex micelles for specific targeting to the tumor neo-vasculature.[15] The RGD peptide (Arg–Gly–Asp) is a recognition motif in multiple ligands of α_v integrins and exhibits an increased affinity to $\alpha_v\beta_3$ and $\alpha_v\beta_5$ integrin receptors,[16] which play a vital role in tumor angiogenesis and metastasis.[17-19] Enhanced cellular uptake and improved intracellular trafficking were achieved in polyplex micelles in the perinuclear region when RGD was conjugated to polyplex micelles, which improved transfection efficiency in HeLa cells possessing $\alpha_v\beta_3$ and $\alpha_v\beta_5$ integrins.[20] In particular, radiolabeled (^{99m}Tc, ^{68}Ga, ^{18}F, ^{64}Cu and ^{111}In) cyclic RGD peptides have been assessed over the last several years as targeted radiotracers for integrin $\alpha_v\beta_3$-positive tumor imaging by tomography techniques such as single photon emission computed tomography (SPECT) and positron emission tomography (PET).[21] Multimeric cyclic RGD moieties were exploited to increase the binding affinity of integrin $\alpha_v\beta_3$ to the radiotracer and were designed to be targeted radiotracers for imaging tumors.[22-24] Furthermore, the radiolabeled uptake (^{99m}Tc, ^{68}Ga, ^{18}F, ^{64}Cu and ^{111}In) of the multimeric cyclic RGD peptides is increased in various normal organs, such as the kidneys, liver, lungs and spleen, which may be due to increased peptide multiplicity.[25] Though it show an appreciably higher tumor uptake with a longer tumor retention time have been attained than their monomeric analogues, stills more efficient, stable and selective integrin $\alpha_v\beta_3$-targeted radiotracers are needed to enhance tumor uptake and increasing tumor-to-background ratio for early diagnosis of integrin $\alpha_v\beta_3$-positive tumors.

Here, we have demonstrated the preparation of targeting polymeric gene carriers based on dimeric cyclic RGD binding PEG-*g*-PEI, (E[c(RGDyK)]$_2$-PEG-*g*-PEI) based polyplexes, and evaluated their ^{99m}Tc-labeled complex as a new radiotracer for *in vivo* studies. The PEG links were used to improve the radiotracer excretion kinetics from noncancerous organs, such as kidneys, liver and lungs. In particular, ^{99m}Tc labeling is an essential focus due to its optimal

nuclear characteristics such as half-life, low-cost abundance and γ-photon energy. The biophysical characterization of radiolabeled polyplexes was evaluated through various methods, including determination of the condensation efficiency, biodistribution, *in vitro* stability and *in vivo* application of the polymers. These properties were studied as function of time in 3D-SPECT/ CT images and by end-point scintillation counting.

Materials and Methods

Materials and Reagents

Branched polyethylenimine [*b*-PEI, molecular weight 25,000 Dalton] was purchased from Sigma-Aldrich. Methoxy poly(ethylene glycol)-N-hydroxysuccinimide [mPEG-NHS, molecular weight 2280 Dalton] and N-hydroxylsuccinimide-PEG-Maleimide [NHS-PEG-MAL, molecular weight 2100 Dalton] were received from Creative PEG Works, Taiwan. Ethidium bromide (EtBr), agarose, uranyl acetate [UA], 3-(4,5-dimethylthiazol-2yl)-2,5-diphenyl-tetrazolium bromide (MTT) and stannous tartrate were purchased from Sigma-Aldrich. ^{99m}Tc pertechnetate was eluted from a technetium generator transferred from Global Medical Solutions Taiwan. Other common chemicals and solvents were purchased from Sigma-Aldrich and were used without further purification.

Synthesis of PEG-*g*-PEI

The preparation of the PEG-*g*-PEI copolymer was carried out in one step (Figure S1). The NHS group of monofunctional PEG reacted with the primary amine of PEI in H_2O under the N_2 atmosphere for 24 h. The degree of incorporation of PEG into PEI (i.e., PEGylation) was determined by ^{1}H-NMR from the ratio of the areas peaks corresponding to the -CH_2- protons of

PEI (2.5–3.1 ppm) and PEG (3.3–3.7 ppm). Based on this estimate, copolymers have been prepared for different molar ratios of PEG: PEI of 1:1 (PP1), 3:1 (PP3), and 10:1 (PP10).

Dimeric *c*RGD peptide moieties were introduced to the PEG segment as the terminal group; the product is referred to as E[c(RGDyK)]$_2$-PEG-*g*-PEI (RPP). Another PEGylated polyethylenimine (PEI) copolymer was prepared without peptide moieties as end groups and is referred as PEG-*g*-PEI (PP).

Synthesis of E[c(RGDyK)]$_2$-PEG-*g*-PEI

The synthesis of E[c(RGDyK)]$_2$-PEG-*g*-PEI (RPP) is a three-step reaction (Figure S2). In the first step, the amino group of the lysine residue of E[c (RGDyK)] $_2$ was altered to a thioacetyl group via reaction with Traut's reagent in HEPES buffer (20 mM HEPES, 150 mM NaCl, 1 mM EDTA, pH 7.2) with various molar ratios from 1 to 5. The reaction mixture was incubated under argon at room temperature for 2 h. In the second step, NHS-PEG-maleimide was subsequently mixed with a certain amount of PEI under argon for 4 h in HEPES buffer. The thioacetyl group of the E[c(RGDyK)]$_2$ was reacted with the maleimide group of the PEG-*g*-PEI under argon overnight. Both the PP and RPP products were purified by centrifugal filtration (10,000 MWCO, Millipore), washed with H_2O for 15 min and lyophilized to a dry powder.

Formation of polyplex

Polyplexes were prepared with PEG-*g*-PEI and plasmid EGFP (*p*EGFP) at different N/P(w/w) ratios, such as 0.1, 0.2, 0.5, 1, 2 and 5. The N/P ratio is the polyplex composition measured as the total weight of the polycation to the weight of *p*EGFP. After gently vortexing the sample, PEG-*g*-PEI/pEGFP (PP/D) polyplexes of a uniform size were formed and then incubated for 30 min.

Characterization of copolymer

The composition of the prepared PEG-*g*-PEI copolymers was estimated using ^{1}H NMR (Bruker AM-500 NMR). The particle sizes and the PEI/D, PP/D and RPP/D zeta potentials were measured using dynamic light scattering (DLS, Zetasizer 3000HS). The morphology of PEG-*g*-PEI/DNA polyplex gene delivery vehicles was observed using a Hitachi H-600 transmission electron microscope. To understand the interaction ability between the positively charged *b*-PEI and the negatively charged *p*EGFP with different N/P ratios, a gel retardation assay using electrophoresis was performed. Aliquots of the solution were taken and assayed by electrophoresis through a 0.7% agarose gel at 80 V for 40 minutes, and the DNA was visualized on a UV transilluminator (or UV box) after immersing the gel in ethidium bromide (EtBr) solution. The cell viability assay studies were evaluated according to a previously reported method.[26] Flow cytometry was performed as described by Ogris et al.[27] All animal experiments were performed in compliance with the guidelines of the Animal Committee of the National Tsing Hua University and all experimental protocols were approved by the Animal Committee of the National Tsing Hua University but human consent had not been used.

In vitro Transfection

100,000 cells per well were seeded in the 6-well plates which would reach 70–80 % confluence onto transfection one day later. A certain amount of PEI, PP and RPP were added to the PBS solution with a fixed amount of plasmid DNA, followed by gentle vortexing for 30 seconds. The resulting solution was incubated at room temperature for 30 minutes and then diluted with growth medium to different concentrations. Before transfection, the old medium was removed from the 6-well plates, followed by washing with PBS three times. Then the polyplex

was added and incubated at 37°C under 5% CO_2 atmosphere for 24 h or 48 h. The fresh growth medium containing 10% FBS was added. The cells were incubated for 24 h in an incubator at 37°C in 5% CO_2. Then the cells were washed once with PBS and then detached with 0.25% trypsin/PBS. Transfection efficiency was evaluated by measuring the percentage of cells expressing GFP (represent Gmean value) using a FACSCanto™ System (Becton-Dickinson, San Jose, CA). Fluorescence parameters from 10,000 cells were acquired. The transfection experiments were carried out in triplicate. The GFP expression was directly visualized under the fluorescence microscope after autofluorescence subtracted.

PP/D and RPP/D polyplex binding assay by flow cytometry

To understand the binding abilities of the PP/D and RPP/D polyplexes, the fluorescent polyplexes were used to detect the binding signals with a FACSCanto™ System by using the signal of the cyanine dyes 7 (Cy7) with ex/em: 743 nm/767 nm as the binding signal, while the GFP signals, ex/em: 395 nm, 475 nm/509 nm, were utilized for the reporter gene expression. Cell binding and uptake efficiency were evaluated by measuring the percentage of cells expressing Cy7 using a standard filter of Alexa Fluor® 700 in the FACSCanto™ System. Fluorescence parameters from 10,000 cells were acquired, and the studies were carried out in triplicate.

Radiolabeling polyplexes with ^{99m}Tc

To a lyophilized vial containing strong ligand (i.e., PEI), 0.1 mg of stannous tartrate in 1 ml of H_2O was added and mixed under N_2. Immediately, a [^{99m}Tc] sodium pertechnetate solution (40 mCi) in 0.9% saline was added. After adding $^{99m}TcO^{4-}$, Tc^{7+} is reduced by Sn^{2+} ions, and the reduced ^{99m}Tc readily forms a chelate with the weaker ligand, i.e., ^{99m}Tc-tartrate. Then, the

stronger ligand (PEI) readily reacts with ^{99m}Tc-tartrate by ligand exchange to form ^{99m}Tc-polyplex. Radiochemical purity and radiolabelling efficiency was measured using silica-gel impregnated glass fiber instant thin-layer chromatography (ITLC-SG) by using acetone as the mobile phase, and the radioactivity was counted using an automatic gamma counter (1470 WIZARD). The PEG-*g*-PEI/*p*EGFP-^{99m}Tc or E[c(RGDyK)]$_2$-PEG-*g*-PEI/*p*EGFP-^{99m}Tc polyplexes (PP/D-^{99m}Tc or RPP/D-^{99m}Tc), which have large molecular weights, would remain at the origin while the pertechnetate moves with the mobile phase at the solvent front.

Radiolabeling stability

The stability of the ^{99m}Tc labeled polyplexes in physiological saline and rat plasma was determined at different time intervals using ITLC-SG. The ^{99m}Tc labeled polyplexes were mixed in saline for 30 minutes, 0.1 ml of the solution (about 0.5-1 mCi) was withdrawn and 0.9 ml of saline or plasma was added in a 1 ml vial. The solution mixture was incubated in saline at room temperature for a period of time from 3, 6, to 24 h. On the other hand, the same solution were prepared and incubated in rat plasma at 37°C for a period for time from 3, 6, to 24 h. After being incubated for different times, the ^{99m}Tc labeled polyplexes solutions in saline or plasma were checked for radiochemical activities using an automatic gamma counter.

NanoSPECT/CT imaging

A high-resolution dual-modality system NanoSPECT/CT (Bioscan, Inc., Washington, DC) imaging, equipped at Chang-Gung Memorial Hospital, Linkou, Taiwan, was used for the animal imaging study. This system features helical scanning for both single-photon emission computed tomography (SPECT) and CT acquisitions using a translation stage with variable axial scanning range from 30 to 180 mm. The static SPECT/CT imaging was taken for whole body

scan with 24 projections and every projection acquired signal within 60 seconds. A total of three mice were respectively injected intravenously into the tail vein each with 1-2 mCi/0.2 ml and 40 μg of ^{99m}Tc-labeled polyplex. The mice were anesthetized with 1.5% isoflurane, positioned prone in the scanner, and performed with nanoSPECT/CT imaging at 1, 3, 6, and 24 h after intravenous injection via the tail vein. All SPECT images were reconstructed using the iteratively ordered subset expectation maximization method from overlapping projects.

Image analysis

Images were viewed and quantified using PMOD image analysis workstation (PMOD Technologies Ltd., Zurich, Switzerland): three-dimensional regions of interest (ROI) on the CT images were drawn around the liver, kidney, lung, heart, spleen, bone, and tumor on decay-corrected whole-body coronal images. The average radioactivity concentration (accumulation) within a tumor or an organ was obtained from mean pixel values within the ROI volume, which were converted to counts per millimeter per minute by using a conversion factor. Assuming a tissue density of 1 g/ mL, the counts per gram per minute and then divided by the injected dose (ID) to obtain an imaging ROI-derived percent injected dose per gram of organ or tissue (%ID/g or %ID/cm^3).

Results and Discussion

Syntheses and characterizations of PEG-*g*-PEI and E[c(RGDyK)]$_2$-PEG-*g*-PEI copolymers

RGD-peptides are good targeting ligands for the tumor endothelium using polyplexes containing siRNA and *p*DNA. Assorted pathogenic organisms were used for an integrin targeting approach by using an integrin receptor to promote their cellular internalization.[18, 28] Although RGD-PEG-PEI has been observed to efficiently deliver nucleic acids into tumors, it has not

demonstrated the enhanced uptake with modulated intracellular trafficking that was observed with cRGD.[29] Thus far, RGD-mimetics have been used as therapeutic agents such as angiogenesis inhibitors, imaging tracers for atherosclerotic plaques, inhibitors for macrophages and enhancers of osseointegration.[30, 31] Here, we describe the synthesis of an RGD-conjugated PEG-*g*-PEI copolymer with different molecular compositions.

The formation of the PEG-*g*-PEI copolymer with different ratios of PEG to PEI was confirmed and the compositions of each fraction were determined using ^{1}H-NMR; the results are shown in Figure 1. The peak at approximately 2.5–3.1 ppm corresponds to PEI hydrogens and the peaks at approximately 3.3–3.7 ppm are attributed to PEG and reveal the existence of both PEG and PEI in the copolymer. The molar ratios are calculated by counting the number of hydrogens both on PEI at 2.5 –3.1 ppm and on PEG at 3.3–3.7 ppm. Accordingly, three different copolymers with PEG/PEI ratios close to 1:1, 3:1, and 10:1 are shown in Table 1. The cRGD conjugated PEG-*g*-PEI copolymer was synthesized, consisting of a 25 kDa molecular weight PEI as the core and a heterobifunctional PEG linker for the PEGylation. PEG was decorated with cRGD molecules at the distal end of the PEG chains, as shown in Figure 1b. Coupling of NHS-PEG maleimide to PEI in HEPES buffer was confirmed by ^{1}H NMR, and the degree of coupling was determined to be approximately 99% of the feed. Hence, conjugation of cRGD to activated PEG depended on both an excess of cRGD moieties and the amount of PEG-linker present. To prepare cRGD-conjugated PP, a 5-fold molar excess of PP and a 4-fold molar excess of RGD were used, resulting in a conjugate designated as E[c(RGDyK)]$_2$-PEG-*g*-PEI (RPP). Similarly, E[c(RGDyK)]$_2$-PEG-*g*-PEI copolymers were identified by the presence of a peak at 7 ppm due to the tyrosine hydrogen of the E[c(RGDyK)]$_2$ moiety. The molar ratio of PEG to E[c(RGDyK)]$_2$

was calculated to be 19.6 from the integrated number of hydrogens at 3.3–3.7 ppm and at 7 ppm in the ^{1}H-NMR spectra.

Formation of PEG-*g*-PEI/DNA polyplexes

PEGylated PEIs and cRGD-modified PEI copolymers are known to be capable of forming polyplexes with *p*DNA. Obviously, the polyplex complex formation can be influenced by the spatial orientation of the targeting moiety. This orientation may be toward the surface of the complexes, resulting in the formation of spherical particles. Polyplex self-assembled micelles were prepared by mixing each polymer solution with the *p*DNA solution at various N/P ratios. The N/P ratio was calculated based on the number of amino groups on the polymer participates in DNA condensation. To demonstrate the interaction ability between positively charged *b*-PEI and negatively charged *p*EGFP with different N/P ratios, a gel retardation assay was performed using 0.7% agarose gel. The movement of the plasmid in the gel would be slowed as the amount of the PEG-*g*-PEI increased, owing to the neutralization of negative charges on the DNA bound in the polymer. At N/P ratios exceeding the ratio for sufficient neutralization, the formed polyplex would migrate slightly toward the anode, providing evidence that it is positively charged. Polyplexes were prepared with PP and *p*EGFP at different N/P ratios: 0.1, 0.2, 0.5, 1, 2 and 5. EtBr have been used to produces a strong fluorescence signal when intercalating with DNA. When DNA is condensed by conjugation with a polycation, ethidium bromide cannot intercalate with DNA. Upon the *p*DNA condensation, decreased fluorescence emission has been obtained due to the coil-to-globular structural transition, and the globular structure inhibits the intercalation of DNA by EtBr. Hence, EtBr exclusion assay have been used to determine the condensation degree of *p*DNA at different N/P ratios quantitatively. As shown in Figure 2, the band of free *p*DNA disappeared at N/P ratio of 0.5 in all of the samples, indicating successful

and complete polyplex formation between *p*DNA and the polycation. Additionally, PEG side chains had no significant effect on the polyplex formation between the PEI main chain and the anionic *p*DNA.

Polyplexes are aggregates and have to be evaluated in the context of surface charge. Therefore, zeta potential measurements can provide sufficient information about polyplex formation by the plasmid and the PP, owing to the neutralization of negative charges on the DNA bound to the positively charged polymer backbone. The zeta potentials of PP/DNA polyplexes at different N/P ratios were measured in H_2O and are shown in Figure 3. The zeta potentials of the polyplexes increased with increasing N/P ratios but showed slight difference at high weight-weight ratio. A more positive surface charge is observed in PP polyplexes with higher N/P ratios due to the shielding effect by nonionic PEG.[32] Most likely, PEG moieties react with the 2° amines of PEI, while copolymerization with 3° amines is hindered due to their high electron density and lower steric hindrance. With PEGylation, the chance to protonate is lower than that observed for 2° amines due to the conversion from 2° amine to 3° amines. Thus, variation in the surface charge of polyplexes may be controlled by decreasing the degree of protonation.

The polyplexes synthesized with N/P ratios of 0.1 and 0.2 exhibited net negative charges because the concentration was insufficient to form a complex and condense DNA. While at 0.5 N/P w/w ratios all polyplex shows positive zeta potential, which is revealed that all DNA are condensed in polycation of PEI. This finding also supported with the result obtained from electrophoresis analysis and confirmation for successful and complete polyplex formation at 0.5 N/P weight ratios as shown in Figure 2. Thus, for the formation of polyplexes with an integral

morphology and a lower positive charge have been obtained when N/P ratio = 1, which was selected for generating the efficient PP/DNA polyplex for further analysis.

Cell Viability Assay

High-molecular-weight PEI (approximately 25 kDa) is significantly more toxic than low-molecular-weight PEI; [33] however, high-molecular-weight PEI has a higher transfection efficiency than low-molecular-weight PEI. To decrease the toxicity of high-molecular-weight PEI, the introduction of PEG to modify PEI is an effective method. Thus, PEGylation is known to help reduce the cytotoxicity of PEI by decreasing the number of PEI amino groups.[34] Moreover, PEI was proven to effectively condense pEGFP, while the formation of the polyplex and the stability of the complex depended on the degree of PEG grafting.[35] To investigate the cytotoxicity of the PEI and PP copolymers, cell viability was determined at different concentrations in HeLa cells. Free polymers were used to measure the cytotoxicity rather than DNA complexes owing to the reduced toxicity that may be obtained by the formation of DNA polyplexes.[36] The cytotoxicity of PEI and PP copolymers at different concentrations in HeLa cells were evaluated (Figure 4). It was found that the cell viability decreased drastically when the concentration of 25 kDa PEI, and PP copolymer was increased from 0.01 to 0.05 mg/ml, whereas approximately >85% of the cell viability could be maintained at a low concentration of PEI and PP copolymer, i.e., less than 0.01 mg/ml. At a high concentration (0.05 mg/ml) of either PP1/D or PP3/D, the cell viability decreased to about 70%, whereas PEI/D shows <40% cell viability. At all concentration (0.01-0.05mg/mL), PP10/D shows high cell viability, i.e., above 89%. As shown in Figure 4, cell viability was follows the orders as PP10/D > PP3/D > PP1/D > PEI/D, which is revealed that the toxicity of PEI was apparently correlated with the degree of PEG grafting and that PP10/D complexes show high cell viability.

Transfection efficiency of the PEG-*g*-PEI/DNA polyplexes

The transfection efficiency from flow cytometry was determined by detecting the fluorescence intensities (Gmean) of the cells. As seen from Figure 5, PP10/D showed the highest transfection efficiency compared to the other two polyplexes with a concentration of 0.025 mg/ml. It was a surprise that PEI/D at 0.025 mg/ml showed much lower transfection efficiency, although it had a high transfection capability due to its inherent polycation nature. This polycation polymer had aroused the death of the cells suspended in the medium, apparently due to its high toxicity. The dead cells were excluded from the flow cytometry count because of its nonspecifically bind with many reagents, which can lead to false positive results. In addition, dead cells may also uptake fluorescent probes since their membranes are permeable to reagents and generate artifacts results.

The toxicity of PEI would reduce the transfection efficiency, as evidenced by the fact that a lower concentration (0.01 mg/ml) resulted in a higher transfection efficiency compared with the concentration of 0.025 mg/ml. The transfection efficiency was clearly affected by the PEG/PEI ratios of the polyplexes; the higher ratio case, i.e., PP10/D, showed much higher efficiency (about 68%), indicating the PEG to PEI sheltering effect.[26] As expected, it was demonstrated that higher concentrations of the polyplex correlated with higher transfection efficiency. Thus, PEI, PP1 and PP2 complexes exhibited lower transfection efficiency compared to PP10 due to sheltering effect from sufficient PEG segments to PEI segments. At low concentration (0.005-0.001mg/mL), transfection efficiency of all polyplex was decreased, which may due to insufficient condensation and protection of DNA inside the complex.

Morphology and size of the PEG-*g*-PEI/DNA polyplexes

The size and shape of a polyplex is acknowledged to be one of the major factors in transfection efficiency. As shown in Figure 6, the size of the self-assembled PP/DNA polyplex is compared with the polymers by measuring their hydrodynamic diameters. The particle sizes of both the PEI- and PP-based polyplex are quite similar, and the copolymerization of PEI does not affect their self-assembled properties with the addition of *p*DNA. Thus, the particle sizes of the polyplexes with different PEG/PEI ratios but the same N/P ratio of 1 were apparently similar over the range of 90 to 140 nm, which may reveal that the N/P ratio and the PEG/PEI ratio would not be the key factors for determining the particle size of the synthesized polyplexes. Interestingly, the cRGD-modified PP-based polyplex (RPP10/D) seemed to have a larger particle size of approximately 135 nm due to the larger size of the cyclic RGD, which may influenced by the protonation profile of the PEI segments, the protonation of the targeting ligand and their interaction with polyanions. Moreover, coupling of PEG decreased the electrostatic interaction of PEI with the negatively charged DNA, which seemed to decrease the size of the polyplexes. The morphology of PP/DNA polyplexes was spherical, as evidenced by the TEM results shown in Figure 6b.

Cell binding assay

Because previous studies showed that the PP10 copolymer had high transfection efficiency and high viability, this copolymer has been conjugated with E[c(RGDyK)]$_2$ to render it a targeting gene delivery carrier; the conjugated product is referred to as RPP10. To confirm the specific cell binding and transfection efficiency of RPP10, a parallel assay for cell binding using PP10 and RPP10 was carried out with flow cytometry, and the results are presented in Figure 7. PP10/D and RPP10/D were prepared at a concentration of 0.025 mg/ml of either copolymer or DNA (N/P=1) and labeled with the fluorescein Cy7. After incubation of PP10/D-

Cy7 or RPP10/D-Cy7 with HeLa cells for 1, 3, and 18 h, the binding of PP10/D-Cy7 and RPP10/D-Cy7 in the cells was analyzed via cell binding signals; the binding of RPP10/D-Cy7 was significantly higher than that of PP10/D-Cy7 (Figure 8a). As presented in Figure 8a, the left black peak was from a control maintained at a low fluorescence intensity, the middle green peak was from the cells accumulated with PP10/D-Cy7, and the right red peak was from the cells accumulated with RPP10/D-Cy7. The results indicated that the gene vector with the E[c(RGDyK)]$_2$ targeting ligand could enhance the binding ability of the HeLa cells. To compare the binding ability and transfection efficiency of RPP10/D with PP10/D, the HeLa cells were subsequently incubated with PP10/D-Cy7 and RPP10/D-Cy7 for 18 h, and GFP expression signals were detected by flow cytometry. It was seen from the results Figure 8b that the binding ability of the cells with RPP10/D was higher than that of the cells with PP10/D. Polyplexes are exposed to high local concentrations of charged macromolecules when they interact with cells, demonstrating that competitive binding with polycations and polyanions within the cell can weaken the polyplexes and cause nucleic acid to be released within the cell. For that reason, GFP expression signals of gene vectors with the E[c(RGDyK)]$_2$-conjugated RPP targeting ligand could enhance the transfection efficiency. All of these results demonstrated that RPP10/D can transport DNA into the cells effectively and might be utilized as an efficient gene delivery vector.

Radiolabeling of PP10/D and RPP10/D by ^{99m}Tc

Radiochemical purity and radiolabelling efficiency was measured using silica-gel impregnated glass fiber instant thin-layer chromatography (ITLC-SG). Radiolabeling efficiencies of PP10/D and RPP10/D with ^{99m}Tc was analyzed and shown to be 96.87% and 98.54%, respectively. The radiochemical stabilities of PP10/D-^{99m}Tc and RPP10/D-^{99m}Tc during

incubation in normal saline at room temperature and in rat plasma at 37 °C are summarized in Table 2. PP10/D-^{99m}Tc and RPP10/D-^{99m}Tc in either condition retained more than 90% radiochemical purity after incubation for 6 h and more than 80% radiochemical purity after incubation for 24 h. It was confirmed that the facile labeling method could produce PP10/D-^{99m}Tc and RPP10/D-^{99m}Tc with high radiolabeling efficiency and high stability in either of PBS or plasma.

Body distribution

RPP10/D polyplexes exhibited significantly higher binding affinity and transfection efficiency (Figure 8) due to effective DNA transportation into the cells. Thus, RPP10/D polyplexes can be identified as promising candidates for local *in vivo* gene transfer due to their improved transfection efficiency. There was a time-dependent change in the distribution of intravenously injected ^{99m}Tc-labeled RPP10/D polyplex complexes in the heart, lungs, liver, kidney, spleen, intestine, blood and brain of female BALB/c nude mice bearing subcutaneous HeLa tumors, as measured through coronal nanoSPECT/CT imaging (Figure 9). The images from left to right are CT, nanoSPECT and nanoSPECT/CT. The tumors were clearly visualized with good contrast in both animal models, and the positions of HeLa tumors are indicated by white arrows. We found that the two tracers of radioactive complexes mainly accumulated in the liver, spleen and kidneys at 1, 3, 6, and 24 h after intravenous injection. Uptake in the spleen and the liver is a common feature of the distribution of the nanoparticles in mice, as studied previously, [37] due to large concentration of macrophages which are parts of the reticuloendothelial systems (RES).

The coronal nanoSPECT/CT images of the two tracers showed the accumulations in the tumor at 1 h after intravenous injection. The coronal nanoSPECT/CT images of RPP10/D-^{99m}Tc showed accumulations in the tumor until 24 h. In contrast, the coronal nanoSPECT/CT image of PP10/D-^{99m}Tc showed almost no accumulation in the tumor at 24 h post-injection. To reduce the sacrifices of animals for *in vivo* studies, SPECT/CT imaging was utilized for the biodistribution study. Regions of interest (ROI) of organs or tissues were circumscribed, and the percentages of doses were calculated. The data from the quantitative analysis of the tracer uptakes in the tumors and the other organs or tissues from SPECT imaging are shown in Figure 10. The tumor uptakes observed on the basis of SPECT quantification are 31.1, 19.8 and 14.6 % ID/cm^3 at 1 h for PP10/D-^{99m}Tc in female BALB/c nude mice bearing subcutaneous HeLa tumors in the liver, kidney and spleen tumor, respectively. The tumor uptake value of RPP10/D-^{99m}Tc was higher than that of PP10/D-^{99m}Tc at 1 h after injection and at the subsequent time points post-injection. The accumulation of the two tracers in the lungs was not higher than the accumulations in the heart, liver, kidney and spleen. This means that PP10/D or RPP10/D with PEI being well sheltered by PEG could invade from the lung uptake.[38] We also noticed the fact that the accumulation of the targeting tracer in bone tissues was higher than the accumulations in the heart, lung, liver and spleen at 3, 6 and 24 h. This is in agreement with a previous report.[39] The bone uptake may be due to the expression of $\alpha_v\beta_3$ integrin in the bone, which is targeted by the tracer. In general, the bone imaging agents (e.g., ^{99m}Tc-phosphonate complexes) depend on ion exchange to accumulate in the bone.[40] The gene vector imaging was also observed to be effectively accumulated in the bone, being evidenced as the targeting effect of the E[c(RGDyK)]$_2$-bound copolymer.

The main excretion routes for PP10/D-^{99m}Tc were both urinary and hepatobiliary, but RPP10/D-^{99m}Tc seemed to be mainly excreted via the urinary system. The liver and spleen uptakes for RPP10/D-^{99m}Tc were apparently lower than those for PP10/D-^{99m}Tc. As a result, the average tumor-to-liver ratio was higher for RPP10/D-^{99m}Tc than for PP10/D-^{99m}Tc at every post-injection time point. The average tumor-to-kidney ratio was slightly higher for RPP10/D-^{99m}Tc than for PP10/D-^{99m}Tc at every post-injection time point. The tumor-to-heart (tumor-to-blood pool) ratios for RPP10/D-^{99m}Tc were clearly higher than those for PP10/D-^{99m}Tc at the same post-injection time points, with the highest ratio at 24 h post-injection (Figure S3 and 4). It is revealed from the results that the targeting ligand, E[c(RGDyK)]$_2$, can improve the tumor accumulation and accelerate the clearance of the bound polyplex from the main organs or tissues. Overall, our results demonstrated that the PP10/D-^{99m}Tc and RPP10/D-^{99m}Tc biodistribution trends studied with the targeting ligand E[c(RGDyK)]$_2$ could improve the tumor accumulation, providing evidence of its targeting effect. Hence, RPP10/D can transport DNA into the cells effectively and might be utilized as an efficient gene delivery vector.

Conclusion

The findings of the present study demonstrate the feasibility of using a dimeric cyclic RGD-PEG-*g*-PEI/*p*EGFP polyplex labeled with ^{99m}Tc as a radiotracer for tumor imaging. The polyplex with a high PEG/PEI ratio of 10:1 can condense with DNA effectively as a gene delivery vehicle. PEG-*g*-PEI copolymer, upon conjugation with DNA with a ratio of 1/1 (w/w), was suitable for DNA condensation, as evidenced by agarose gel retardation assay and size and zeta potential measurements. The RPP10/D polyplex exhibited significantly higher binding with the HeLa cells and enhanced gene expression compared with non-targeting PP10/D. The RPP10/D polyplex demonstrated significantly higher binding affinity and transfection efficiency

and exhibited effective endosomal escape properties due to protonation of branched PEI chains with decreasing pH. Polyplexes as molecular imaging probes are observed using SPECT/CT imaging; the uptake of RPP10/D in the tumor was higher than that of PP10/D. The obtained results revealed that the interaction of the ^{99m}Tc-labeled targeting ligand E[c(RGDyK)]$_2$-conjugated PEG-g-PEI with tumor tissue resulted in a strong signal, which means that the tumor uptake of radiotracers in the *in vivo* PET images and biodistribution of the tumor.

Acknowledgements

We are indebted to Ministry of Science and Technology, Taiwan, for financial support (MOST 103-2221-E-033-012-), and thanks Jem-Mau Lo and Jian-Yu Chen for his kindly assistance in this study.

References

1. A. Pathak, S. Patnaik and K. C. Gupta, *Biotechnology journal*, 2009, **4**, 1559-1572.
2. D. Schaffert and E. Wagner, *Gene therapy*, 2008, **15**, 1131-1138.
3. H. Cohen, R. J. Levy, J. Gao, I. Fishbein, V. Kousaev, S. Sosnowski, S. Slomkowski and G. Golomb, *Gene Ther*, 2000, **7**, 1896-1905.
4. D. Luo and W. M. Saltzman, *Nat Biotech*, 2000, **18**, 33-37.
5. A. Dasgupta, P. K. Das, R. S. Dias, M. G. Miguel, B. Lindman, V. M. Jadhav, M. Gnanamani and S. Maiti, *The Journal of Physical Chemistry B*, 2007, **111**, 8502-8508.
6. S. Gawęda, M. C. Morán, A. A. Pais, R. S. Dias, K. Schillén, B. Lindman and M. G. Miguel, *Journal of colloid and interface science*, 2008, **323**, 75-83.
7. S.-Y. Lin, W.-Y. Zhao, H.-C. Tsai, W.-H. Hsu, C.-L. Lo and G.-H. Hsiue, *Biomacromolecules*, 2012, **13**, 664-675.

8. S. C. De Smedt, J. Demeester and W. E. Hennink, *Pharm Res*, 2000, **17**, 113-126.

9. O. Boussif, F. Lezoualc'h, M. A. Zanta, M. D. Mergny, D. Scherman, B. Demeneix and J.-P. Behr, *Proceedings of the National Academy of Sciences*, 1995, **92**, 7297-7301.

10. L. Parhamifar, A. K. Larsen, A. C. Hunter, T. L. Andresen and S. M. Moghimi, *Soft Matter*, 2010, **6**, 4001-4009.

11. S.-Y. Wu, L.-T. Chang, S. Peng and H.-C. Tsai, *International journal of nanomedicine*, 2015, **10**, 1637-1647.

12. M. A. Wolfert, E. H. Schacht, V. Toncheva, K. Ulbrich, O. Nazarova and L. W. Seymour, *Human gene therapy*, 1996, **7**, 2123-2133.

13. S. Mishra, P. Webster and M. E. Davis, *European journal of cell biology*, 2004, **83**, 97-111.

14. A. M. Funhoff, S. Monge, R. Teeuwen, G. A. Koning, N. M. Schuurmans-Nieuwenbroek, D. J. Crommelin, D. M. Haddleton, W. E. Hennink and C. F. van Nostrum, *Journal of controlled release*, 2005, **102**, 711-724.

15. M. Oba, S. Fukushima, N. Kanayama, K. Aoyagi, N. Nishiyama, H. Koyama and K. Kataoka, *Bioconjugate chemistry*, 2007, **18**, 1415-1423.

16. R. Haubner, R. Gratias, B. Diefenbach, S. L. Goodman, A. Jonczyk and H. Kessler, *Journal of the American chemical society*, 1996, **118**, 7461-7472.

17. S. M. Weis and D. A. Cheresh, *Cold Spring Harbor Perspectives in Medicine:*, 2011, **1**, a006478.

18. U. K. Marelli, F. Rechenmacher, T. R. A. Sobahi, C. Mas-Moruno and H. Kessler, *Frontiers in Oncology*, 2013, **3**, 222.

19. J. S. Desgrosellier and D. A. Cheresh, *Nature reviews. Cancer*, 2010, **10**, 9-22.

20. K. Temming, R. M. Schiffelers, G. Molema and R. J. Kok, *Drug resistance updates*, 2005, **8**, 381-402.

21. S. Liu, *Molecular pharmaceutics*, 2006, **3**, 472-487.

22. I. Dijkgraaf, J. A. Kruijtzer, S. Liu, A. C. Soede, W. J. Oyen, F. H. Corstens, R. M. Liskamp and O. C. Boerman, *European journal of nuclear medicine and molecular imaging*, 2007, **34**, 267-273.

23. S. Liu, W.-Y. Hsieh, Y. Jiang, Y.-S. Kim, S. G. Sreerama, X. Chen, B. Jia and F. Wang, *Bioconjugate Chemistry*, 2007, **18**, 438-446.

24. S. Liu, *Bioconjugate chemistry*, 2009, **20**, 2199-2213.

25. J. Shi, Y.-S. Kim, S. Zhai, Z. Liu, X. Chen and S. Liu, *Bioconjugate chemistry*, 2009, **20**, 750-759.

26. G.-H. Hsiue, H.-Z. Chiang, C.-H. Wang and T.-M. Juang, *Bioconjugate chemistry*, 2006, **17**, 781-786.

27. M. Ogris, P. Steinlein, S. Carotta, S. Brunner and E. Wagner, *Aaps Pharmsci*, 2001, **3**, 43-53.

28. J. Kim, S. W. Kim and W. J. Kim, *Oligonucleotides*, 2011, **21**, 101-107.

29. J. T. Connelly, A. J. García and M. E. Levenston, *Biomaterials*, 2007, **28**, 1071-1083.

30. F. Wang, Y. Li, Y. Shen, A. Wang, S. Wang and T. Xie, *International journal of molecular sciences*, 2013, **14**, 13447-13462.

31. F. A. Jaffer, P. Libby and R. Weissleder, *Journal of the American College of Cardiology*, 2006, **47**, 1328-1338.

32. S. K. Cho and Y. J. Kwon, *Journal of Controlled Release*, 2011, **150**, 287-297.

33. M. Mady, W. Mohammed, N. M. El-Guendy and A. Elsayed.

34. L. Wightman, R. Kircheis, V. Rössler, S. Carotta, R. Ruzicka, M. Kursa and E. Wagner, *The journal of gene medicine*, 2001, **3**, 362-372.

35. Y. Kakizawa and K. Kataoka, *Advanced drug delivery reviews*, 2002, **54**, 203-222.

36. K. Kunath, A. von Harpe, D. Fischer, H. Petersen, U. Bickel, K. Voigt and T. Kissel, *Journal of Controlled Release*, 2003, **89**, 113-125.

37. F. Alexis, E. Pridgen, L. K. Molnar and O. C. Farokhzad, *Molecular pharmaceutics*, 2008, **5**, 505-515.

38. E.-M. Kim, H.-J. Jeong, I.-K. Park, C.-S. Cho, C.-G. Kim and H.-S. Bom, *Journal of Nuclear Medicine*, 2005, **46**, 141-145.

39. P. Schaffner and M. Dard, *Cellular and Molecular Life Sciences CMLS*, 2003, **60**, 119-132.

40. O. W. Krogsgaard, *European journal of nuclear medicine*, 1976, **1**, 15-17.

Figure captions

Figure 1. ^{1}H NMR spectra of the synthesized copolymers and RGD-bound copolymer in D_2O: (a) PEG-*g*-PEI (b) E[c(RGDyK)]$_2$-PEG-*g*-PEI.

Figure 2. Agarose gel electrophoresis of PEI/DNA and copolymer/DNA complexes at various N/P ratios. Lane 1, DNA marker [excluded (a)]; Lane 2, N/P= 0 (plasmid only); lanes 3-8, N/P ratio: 0.1, 0.2, 0.5, 1, 2 and 5.

Figure 3. Zeta potential measured for the prepared polyplexes with DNA (PEI/D, PP1/D, PP3/D and PP10/D)

Figure 4. Cytotoxicities of PEI/DNA and copolymer/DNA polyplexes at varying concentrations of 0.001, 0.005, 0.01, 0.025, and 0.05 mg/ml (n=4)

Figure 5. Transfection efficiencies of the polyplexes with different PEG/PEI ratios at varying concentrations of either copolymer or DNA (N/P=1).

Figure 6. (a) Particle sizes of PEI/D and copolymer/DNA polyplexes at N/P=1 (n = 3). (b) A representative image for confirmation of the PP10/DNA polyplexes imaged by TEM.

Figure 7. Cell binding and uptake abilities of PP10/D-Cy7 and RPP10/D-Cy7 by the HeLa cells along with incubation for 1, 3, and 18 h (N/P=1, in 0.025 mg/ml, n=3). Error bars represent SD. *P<0.05; the results for Gmean of RPP10/D are significantly higher than those of PP10/D.

Figure 8. (a) Flow cytometry chromatograms of the HeLa cells incubated with RPP10/D-Cy7 and PP10/D-Cy7 for 18 h. (b) Comparison of the transfection efficiency of RPP10/D with PP10/D from the incubation of the cells with both of the gene vectors for 18 h and Gmean for RPP10/D was higher than for PP10/D (*P<0.05).

Figure 9. Comparison of coronal nanoSPECT/CT images of PP10/D-^{99m}Tc and RPP10/D-^{99m}Tc in female BALB/c nude mice bearing subcutaneous HeLa tumors. The images were acquired at 1, 3, 6 and 24 h after intravenous injection. PP10/D-^{99m}Tc or RPP10/D-^{99m}Tc containing approximately 1.2 mCi of ^{99m}Tc was administered to the mice by intravenous injection. The images from left to right are CT images, nanoSPECT images and nanoSPECT/CT images. The positions of HeLa tumors are indicated by white arrows.

Figure 10. (a) *In vivo* biodistribution data of PP10/D-^{99m}Tc in female BALB/c nude mice bearing subcutaneous HeLa tumors. The values are presented as %ID/ cm^3, mean ± S.D. (b) *In vivo* biodistribution data of RPP10/D-^{99m}Tc in female BALB/c nude mice bearing subcutaneous HeLa tumors. The values are presented as %ID/ cm^3, mean ± S.D. (n = 3 at each time point)

Table captions

Table 1. The molar ratios of PEG/PEI and PEG/RGD of PEG-g-PEI copolymers from the reactants to the products.

Table 2. Stabilities (%) of PP10/D-^{99m}Tc and RPP10/D-^{99m}Tc during incubation in normal saline and rat plasma for 3, 6, and 24 h.

Figures

(a)

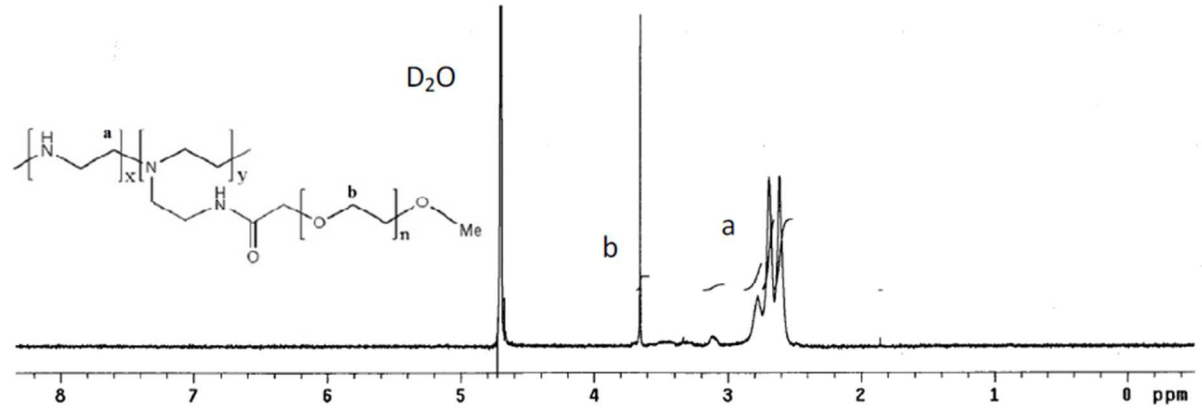

(b)

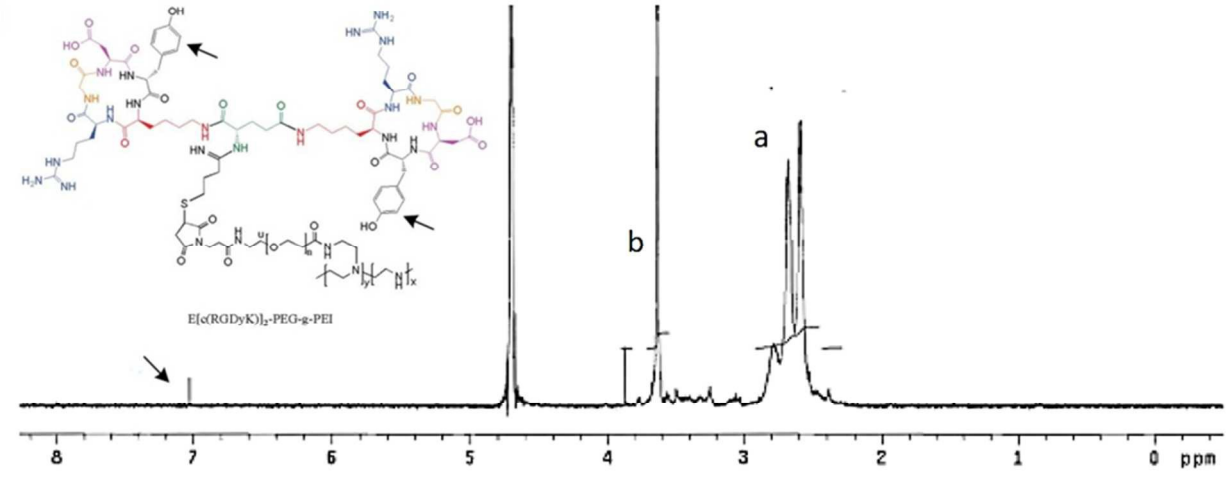

Figure 1

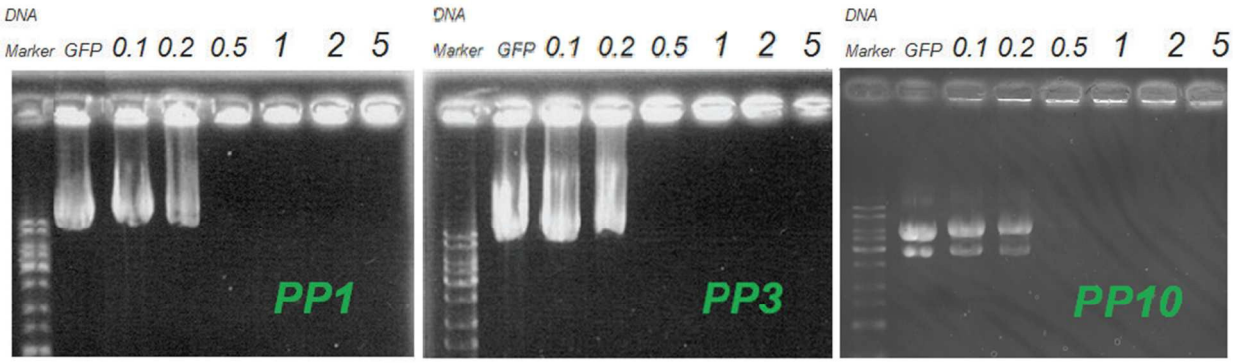

Figure 2

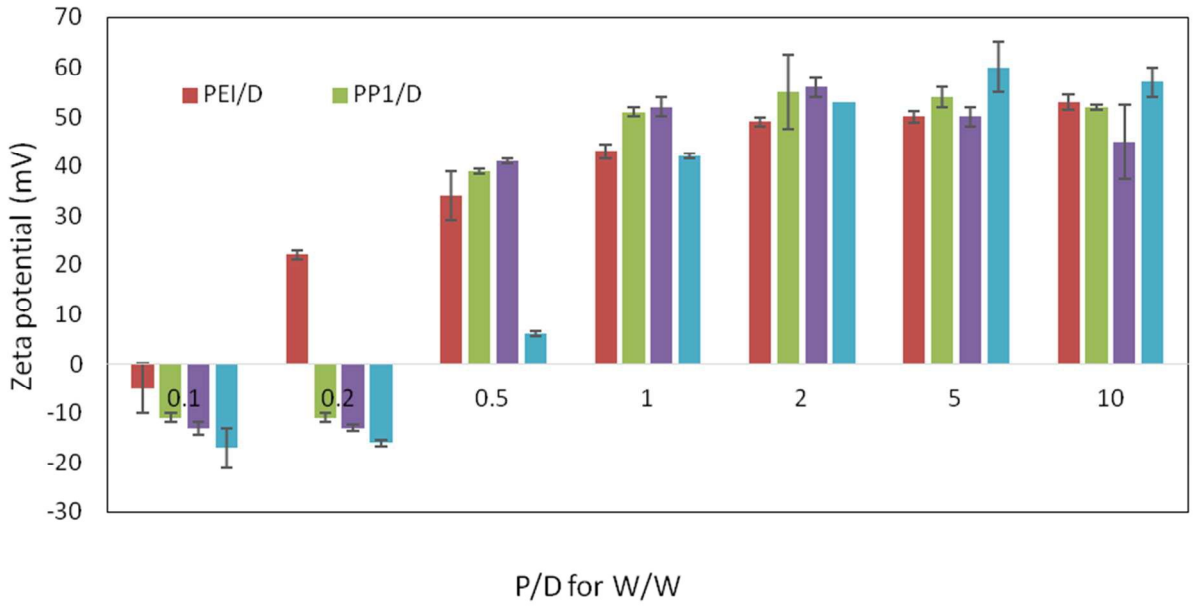

Figure 3

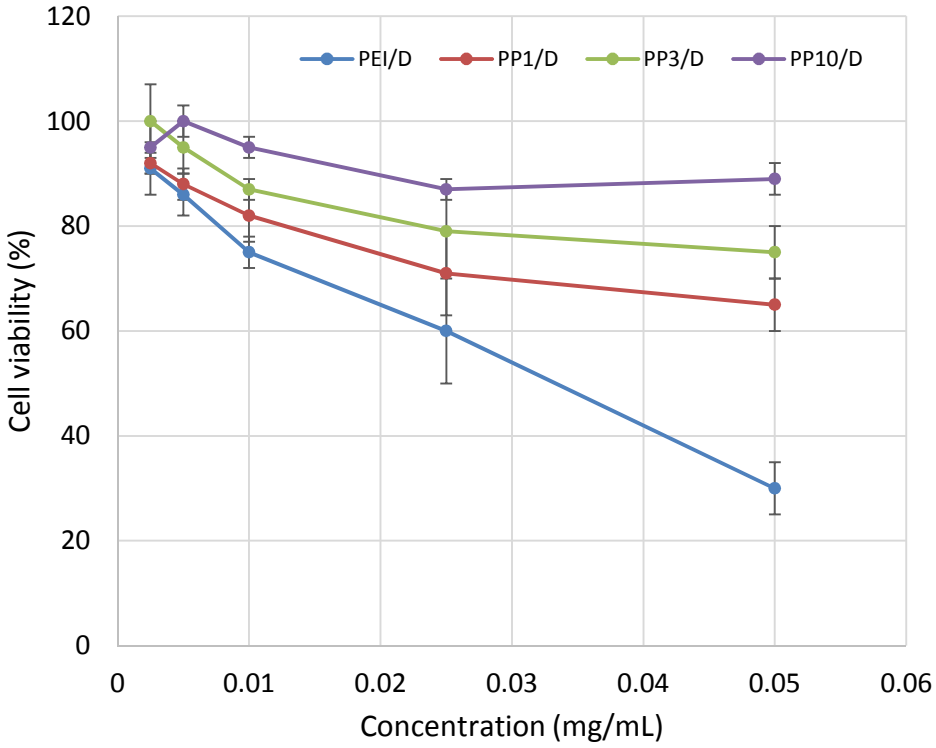

Figure 4

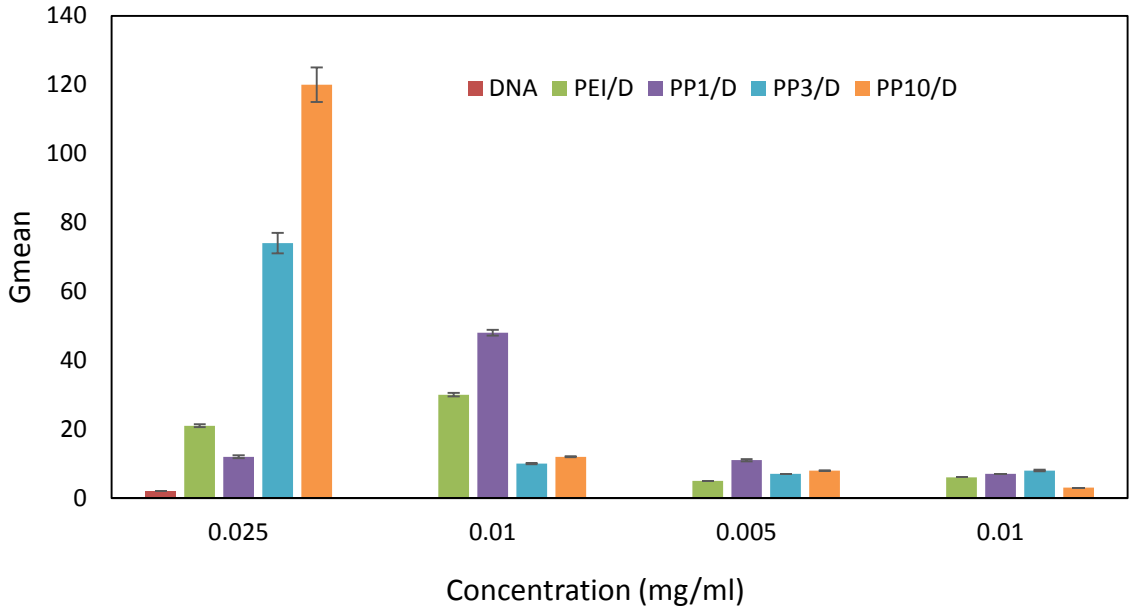

Figure 5

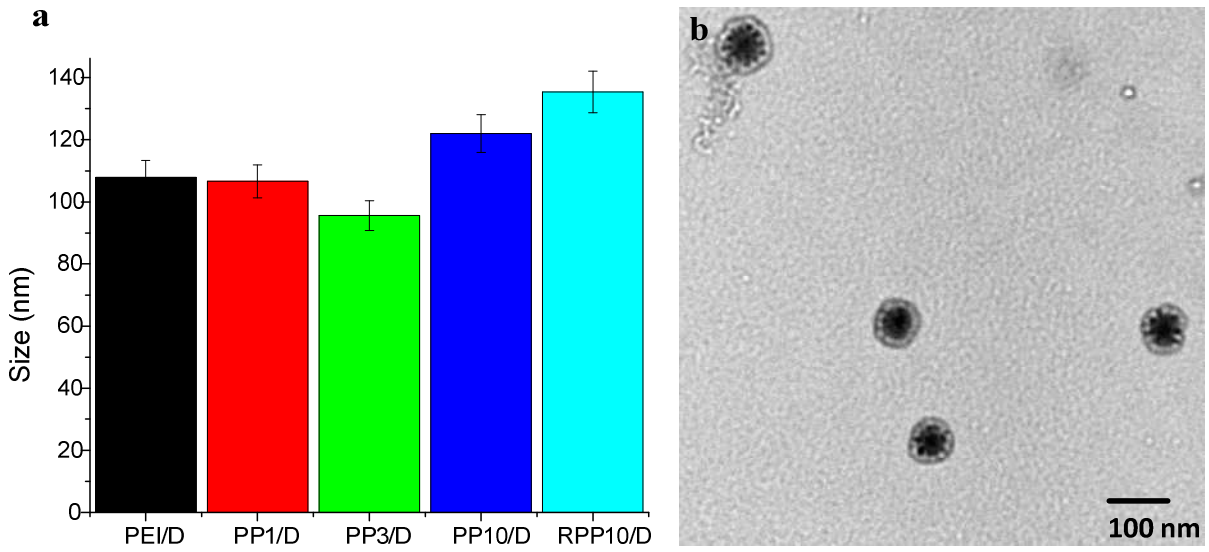

Figure 6

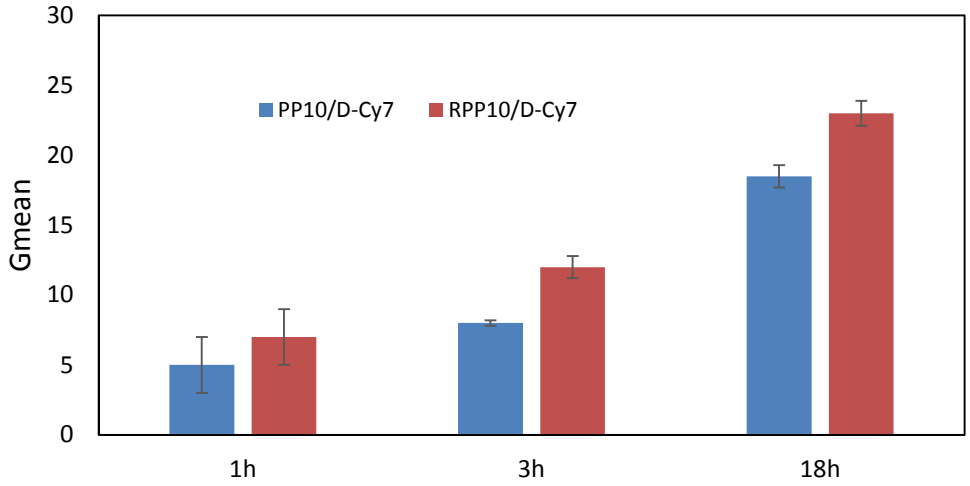

Figure 7

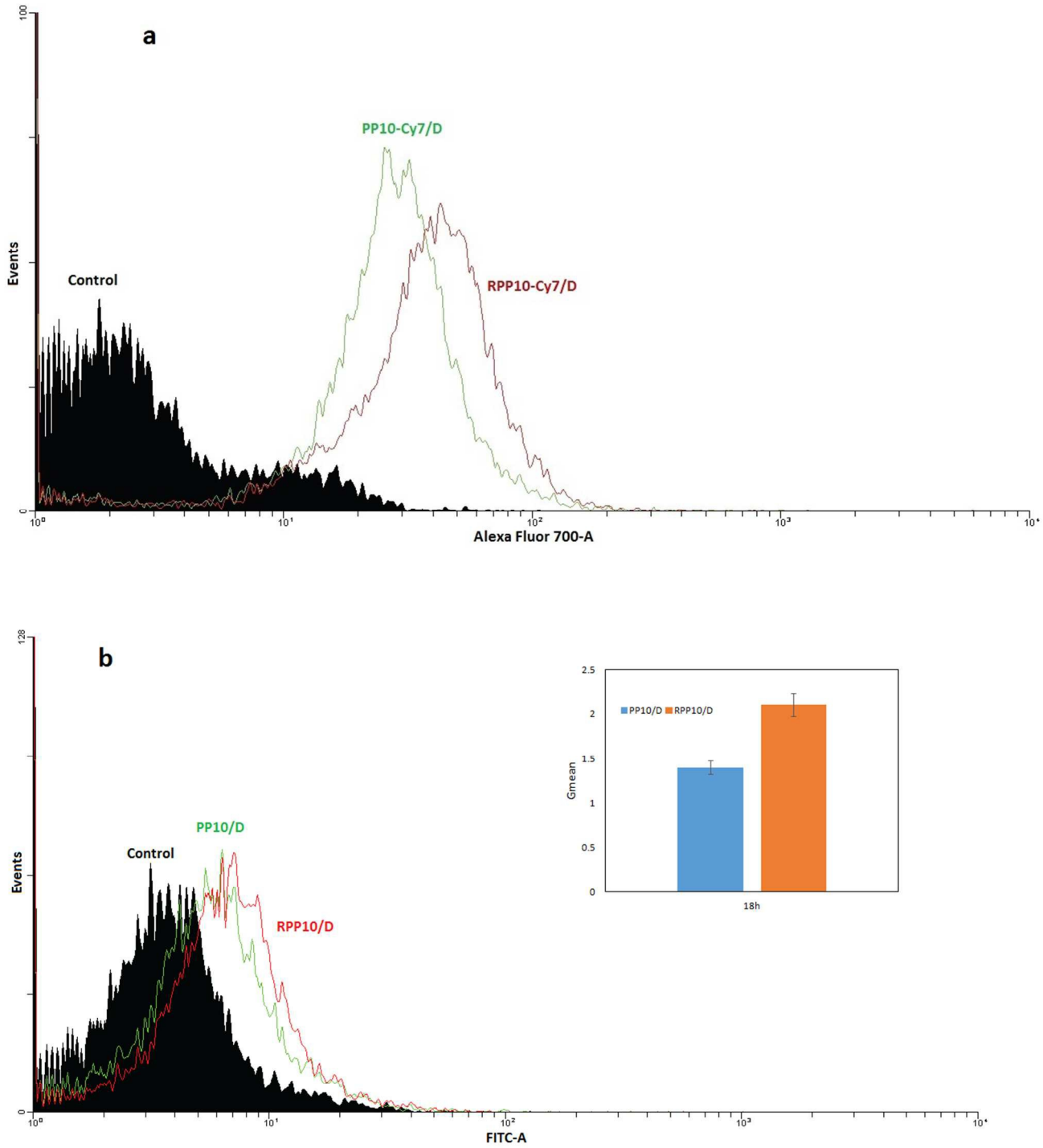

Figure 8

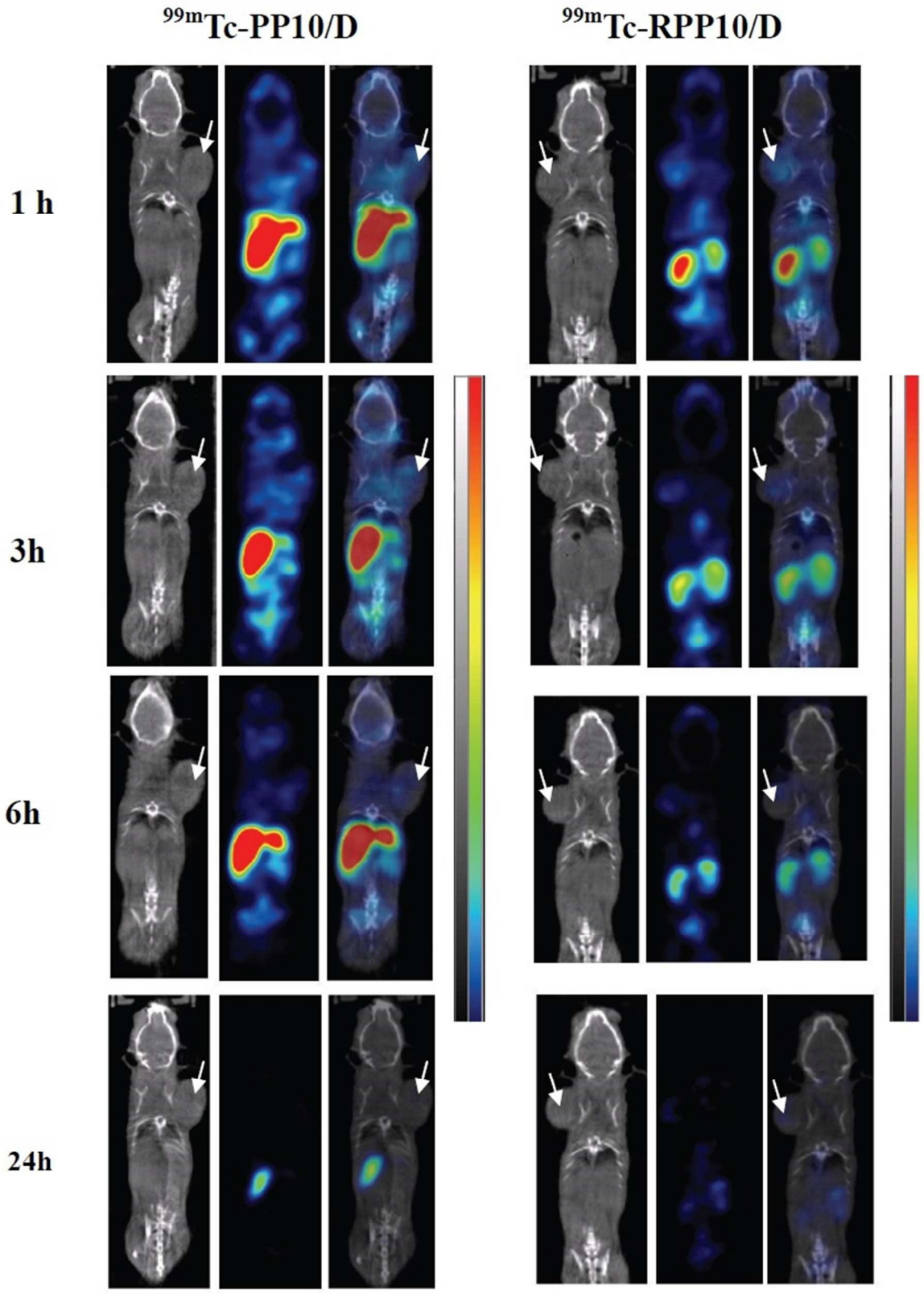

Figure 9

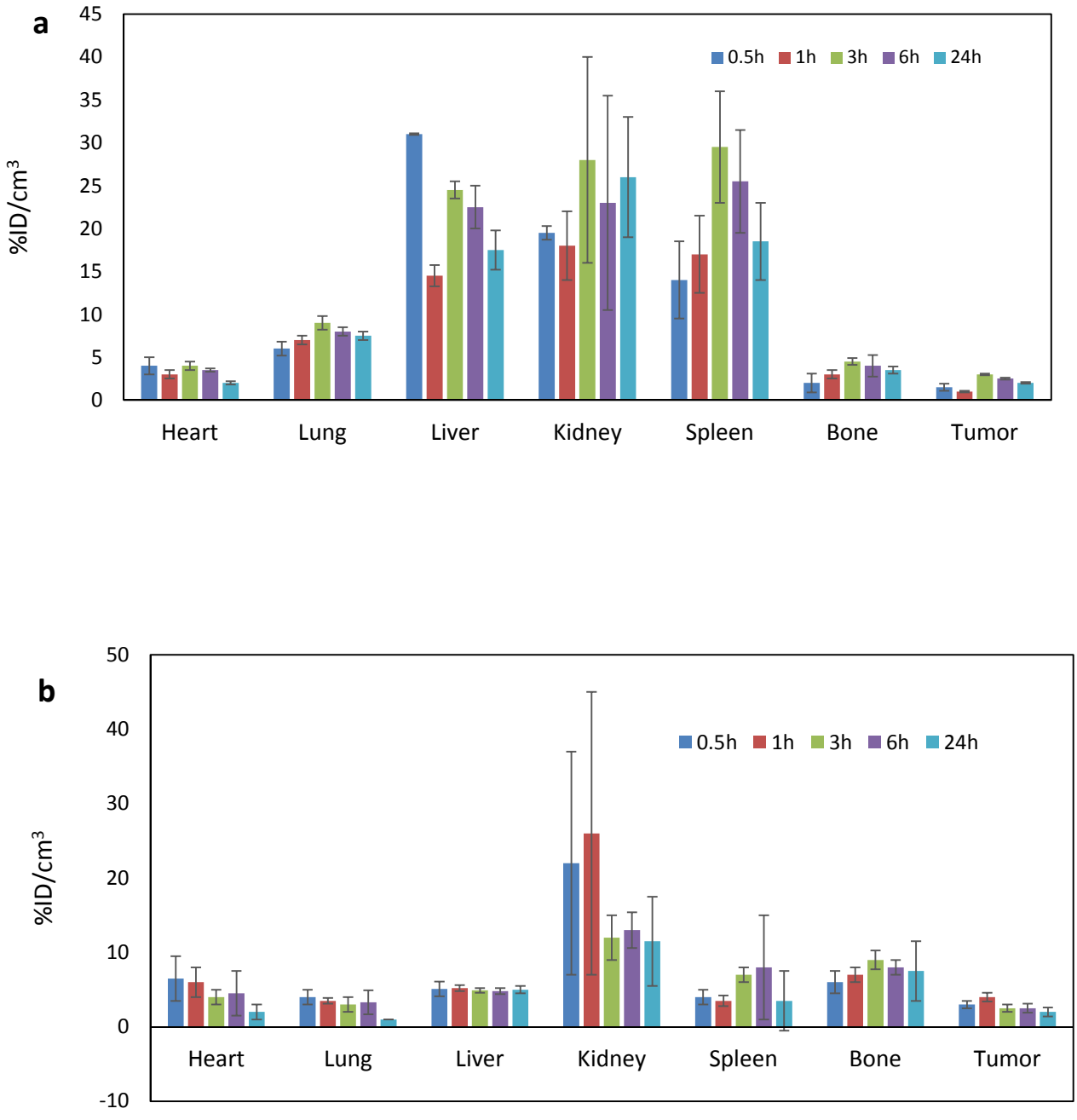

Figure 10

Tables

Table 1. The molar ratios of PEG/PEI and PEG/RGD of PEG-*g*-PEI copolymers from the reactants to the products.

Copolymer	Reaction		Production	
	PEG/PEI (mol/mol)	PEG/RGD (mol/mol)	PEG/PEI (mol/mol)	PEG/RGD (mol/mol)
PEG-g-PEI (PP1)	1	-	1.1	-
PEG-g-PEI (PP3)	3	-	3.6	-
PEG-g-PEI (PP10)	10	-	9.9	-
E[c(RGDyK)]$_2$-PEG-g-PEI (RPP10)	10	8	10.8	19.6

Table 2. Stabilities (%) of PP10/D-^{99m}Tc and RPP10/D-^{99m}Tc during incubation in normal saline and rat plasma for 3, 6, and 24 h

	Incubation Time (h)	3	6	24
PP10/D-^{99m}Tc	in saline	95.93±2.81	95.64±1.72	87.97±5.26
	in plasma	92.14±5.02	90.45±8.92	80.88±6.92
RPP10/D-^{99m}Tc	in saline	97.29±0.16	96.75±0.29	85.66±0.48
	in plasma	96.12±0.98	95.52±2.75	84.21±9.80

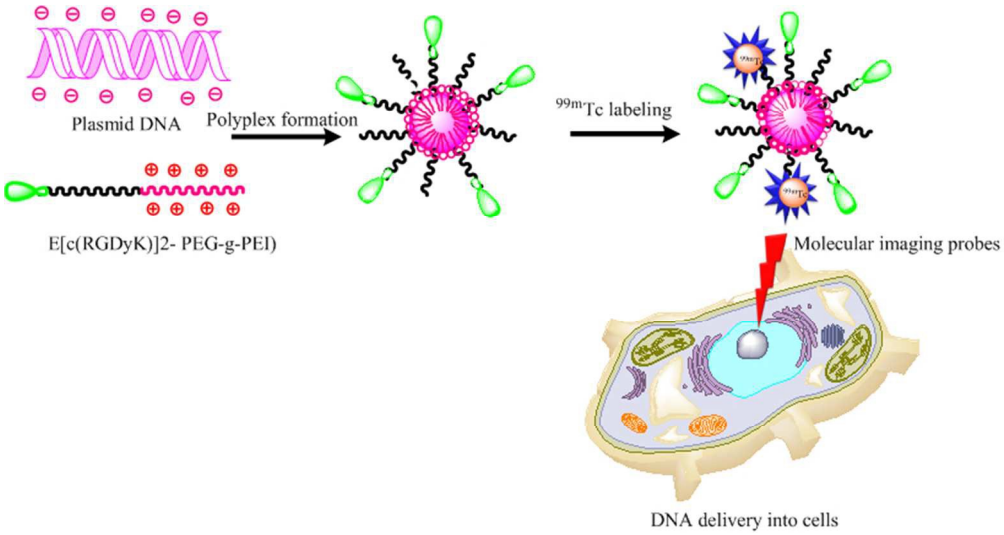

Polyplex micelles with pEGFP and RGD -modified poly(ethylene glycol)-grafted polyethylenimine (E[c(RGDyK)]2-PEG-g-PEI) and were labeled with 99mTc for the in vivo study as proficient probes for molecular imaging.
216x114mm (96 x 96 DPI)